Journal of Solid State Chemistry **156,** 255–263 (2001)
doi:10.1006/jssc.2000.8896, available online at http://www.idealibrary.com on IDEAL®

Crystal Structures and Phase Transitions in the $SrTiO_3$–$SrZrO_3$ Solid Solution

Tony Kam-Yuen Wong and Brendan J. Kennedy

The School of Chemistry, The University of Sydney, Sydney, NSW 2006, Australia

Christopher J. Howard and Brett A. Hunter

Australian Nuclear Science and Technology Organisation, Private Mail Bag 1, Menai, NSW 2234, Australia

and

Tom Vogt

Physics Department, Building 510B Brookhaven National Laboratory, Upton, New York

Received March 31, 2000; in revised form June 29, 2000; accepted July 28, 2000

Laboratory and synchrotron X-ray powder diffraction and neutron powder diffraction have been used to determine crystal structures in the perovskites $SrTi_xZr_{1-x}O_3$. Superlattice reflections in the neutron diffraction patterns proved to be the most reliable indicators of lower symmetry structures. The room temperature structures are orthorhombic *Pbnm* in the range of $0 \le x \le 0.4$, tetragonal *I4/mcm* in the range $0.4 < x \le 0.95$, and cubic $Pm\bar{3}m$ for $0.95 < x \le 1$. Additional measurements were made on the room-temperature tetragonal samples at $x = 0.5$, 0.75, and 0.9. The first two were examined at elevated temperatures, using neutron diffraction methods, where the transition tetragonal to cubic was noted. Measurements at low temperatures using synchrotron X-ray powder diffraction are reported. © 2001 Academic Press

INTRODUCTION

For many years there has been considerable interest in the nature of the crystallographic transitions in perovskite, $CaTiO_3$, and structurally related ABO_3-type metal oxides. There are three main reasons for this, namely: (i) the possibility that $MgSiO_3$, which is the major mineral in Earth's lower mantle, undergoes a series of temperature- and pressure-induced phase transitions (1), and the understanding of these may be of crucial importance in appreciating the geophysical properties of the lower mantle; (ii) $CaTiO_3$ is one of the major phases of Synroc, a titanate ceramic designed for the immobilization of high level radioactive waste (2); and (iii) fundamental investigation of structural instabilities in metal oxides. In the first two areas, the influence of dopants, on either the A-type or the B-type cation sites is of interest. Perovskite type oxides are also well represented in technologically important areas, including high-temperature superconductors (3), giant magnetoresistive oxides (4), and piezo- and ferroelectric oxides (5), where again cation substitutions play a key role in controlling and tuning the desirable properties. The PZT ($PbZr_{1-x}Ti_xO_3$) ferroelectrics are perovskites having two different cations on the B-type site (6).

The system $CaTiO_3$–$SrTiO_3$, investigated recently by Ball *et al.* (7), provides an example of a perovskite system with cation substitution, Ca for Sr, on the A-type site. At room temperature $SrTiO_3$ adopts the ideal cubic perovskite structure $Pm\bar{3}m$ with $a = 3.8$ Å. On cooling below 150 K the structure becomes tetragonal, $I4/mcm$ with $a \approx \sqrt{2}a$ and $c \approx 2a$ (8). By contrast $CaTiO_3$ is orthorhombic, *Pbnm*, at room temperature, $a \approx \sqrt{2}a$, $b \approx \sqrt{2}a$, and $c \approx 2a$, and this transforms to the tetragonal $I4/mcm$ intermediate at 1500 K and finally to the cubic $Pm\bar{3}m$ structure at 1580 K (9). From precise lattice parameter determination and a close examination of the weak superlattice reflections in X-ray synchrotron powder diffraction patterns, Ball and coworkers (7) concluded that the room temperature structures in the system $Ca_{1-x}Sr_xTiO_3$ were orthorhombic in *Pbnm* for $0 \le x \le 0.4$, apparently tetragonal with $c/a < 1$ for $0.45 \le x \le 0.6$, tetragonal in $I4/mcm$ and with $c/a > 1$ for $0.65 \le x \le 0.9$, and cubic in $Pm\bar{3}m$ for $x \ge 0.95$. Ball *et al.* suggested that the apparently tetragonal structure with $c/a < 1$ was in fact orthorhombic in *Cmcm*, bringing the sequence of phases into line with those reported for $SrZrO_3$ (10–12), and suggested more recently for $SrHfO_3$ (13) and for $CaTiO_3$ itself (9), upon increasing the temperature.

Of the four structures mentioned above only the *Cmcm* structure contains two inequivalent A-type cation sites. The

0022-4596/01 $35.00

other three space groups give a single occupied A-type cation site. Woodward (14) has suggested that for perovskites with a single A-type cation a space group with equivalent A sites will be favored. For this reason in both $CaTiO_3$ and $SrZrO_3$ the formation of the *Cmcm* phase can be considered unusual, although in $Ca_{0.5}Sr_{0.5}TiO_3$ the different sizes of the two A-site cations may favor it. We note that to distinguish the *Cmcm* from the more common *Pbnm* structure in these ABO_3 perovskites using powder diffraction methods is far from trivial (7, 9), especially considering that for $CaTiO_3$ and $SrMO_3$ (M = Zr, Hf) the phase is reported to exist only at high temperatures (9–13). It is possible that the reports of the *Cmcm* phase in these three oxides are incorrect. Nor does the group theoretical analysis (15) help in determining the possible occurrence of the *Cmcm* structure. It shows that the transition from tetragonal to cubic can be continuous, consistent with our previous experimental studies (9, 10, 13), but there is no continuous pathway from the orthorhombic *Pbnm* to tetragonal *I*4/*mcm* whether or not an intermediate orthorhombic *Cmcm* is involved. It remains unclear if the transformation proceeds directly from *Pbnm* to *I*4/*mcm* or involves a *Pbnm*–*Cmcm*–*I*4/*mcm* pathway.

Since it is easier to conduct structural studies under ambient conditions than under those of high temperature or pressure, as appropriate in Earth's mantle, or even at the temperature of the tetragonal to cubic transition in $CaTiO_3$ and $SrMO_3$ (M = Zr, Hf) we believe it desirable to establish if the form of the temperature-induced structural transformation can be reproduced by suitable chemical substitutions. In view of this, and as part of our experimental program on perovskites (9, 10, 13, 16–18), we have undertaken studies on the $SrTiO_3/SrZrO_3$ system. This is a system involving cation substitution, Zr for Ti, on the B-type site. The end members $SrTiO_3$ and $SrZrO_3$ are, as already noted, cubic in $Pm\bar{3}m$ and orthorhombic in *Pbnm*, respectively, so the system is expected to provide access to the desired phases at convenient temperatures.

The present paper describes the results of powder neutron and synchrotron diffraction studies directed toward three aims:

1. Determine the nature of the composition-induced tetragonal to cubic phase transition; that is, does it have the same functional form as the temperature-induced transition?

2. Determine the composition-phase relationship in this system.

3. Investigate the possible formation of a *Cmcm* phase, without the complication of two different A-type cations.

EXPERIMENTAL

The $SrTi_xZr_{1-x}O_3$, perovskite-type oxides were prepared by mixing high-purity $SrCO_3$ (Merck), TiO_2 (Aldrich), and ZrO_2 (Townson & Mercer) in the appropriate stoichiometric ratios in an acetone slurry and grinding, using a mortar and pestle, until dry. The homogeneous solid mixtures were then compressed in alumina crucibles and heated in air at 800°C for 24 h, at 1200°C for 24 h, and finally at 1400°C for 96 h with periodic regrinding, mixing, and pressing. Samples were characterized at room temperature, using powder X-ray diffraction patterns recorded on a Siemens D-5000 Diffractometer, using Cu$K\alpha$ radiation. Data were recorded in the range $20^\circ < 2\theta < 110^\circ$ with step size 0.02° and the time per step 10 s. The divergence and anti-scatter slits used were 1.0 mm.

Room-temperature synchrotron X-ray diffraction patterns were collected at the Australian National Beamline Facility (ANBF) diffractometer at the Photon Factory, Tsukuba, Japan (19). The diffraction data were recorded at a wavelength of $\lambda = 0.80005$ Å, in steps of 0.01° on two separate image plates with 2θ ranges from 5 to 45° and 45 to 85°. High-resolution variable temperature synchrotron X-ray diffraction patterns were collected at X7A at the National Synchrotron Light Source at Brookhaven National Laboratory (USA), making use of a linear position-sensitive detector with a spatial resolution of less than 50 μm (20). In all the synchrotron diffraction studies the samples were housed in 0.3–mm-diameter capillaries which, for low-temperature measurements, were mounted in a closed-cycle He cryostat.

The neutron powder diffraction patterns were recorded using neutrons of wavelength 1.664 Å in the range $10^\circ < 2\theta < 138^\circ$ with a step size of 0.10° on the medium-resolution powder diffractometer (MRPD) (21) on the High-Flux Australian Reactor (HIFAR) operated by the Australian Nuclear Science and Technology Organisation (ANSTO). The powdered samples were held in thin-walled 12 or 16-mm-diameter vanadium cylinders. For the high-temperature measurements the samples were placed in 12-mm stainless steel cans and the furnace was open to the atmosphere during the measurements. An additional pattern for $SrTi_{0.5}Zr_{0.5}O_3$ was recorded using neutrons of wavelength 1.4925 Å in the range $10^\circ < 2\theta < 154^\circ$ with the step size of 0.05° on the high-resolution powder diffractometer (22) on HIFAR. For all the powder neutron diffraction measurements the sample was rotated about the vertical axis to reduce the effects of preferred orientation.

The structural refinements were undertaken using the Rietveld program Rietica (23). In the neutron diffraction studies the background was defined by a third-order polynomial in 2θ and was refined simultaneously with the other profile parameters. For the synchrotron diffraction work a 20- to 30-point interpolated background was employed. A Voigt function was chosen to generate the line shape of the neutron diffraction peaks where the width of the Gaussian component was varied according to $(\mathrm{FWHM})^2 = U\tan^2\theta + V\tan\theta + W$ to describe instrumental and strain

broadening and that of the Lorentzian component as $\eta \sec\theta$ to model broadening due to particle size. In structural refinements from the high temperature neutron diffraction studies the iron of the sample holder was included as a second phase.

RESULTS AND DISCUSSION

The structures of the oxides $SrTi_xZr_{1-x}O_3$ were first studied using the laboratory powder X-ray diffraction data. As the amount of Ti present in the material increased there was a reduction in the number of observed reflections, indicating transitions to higher symmetry. Nevertheless, the volume per formula unit decreases continuously upon Ti substitution (Fig. 1). Duplicate points in this figure arise from the use of both X-ray and neutron diffraction data.

At room temperature $SrZrO_3$ has an orthorhombic (*Pbnm*) structure (10, 11) and careful examination of the various weak, superlattice reflections[1] in the powder X-ray diffraction patterns suggested that samples with high Zr contents, $0 \le x \le 0.35$, also exhibited *Pbnm* symmetry. This is best monitored by examining the 021 and 122/212 reflections, near $2\theta = 33$ and 41° (Cu$K\alpha$ radiation) or 17.0 and 21.5° (Synchrotron 0.8 Å), respectively. This space group was confirmed by successful structural refinements using the Rietveld method, and final parameters for samples near the *Pbnm*–*I*4/*mcm* interface are listed in Table 1. The final refinements of the orthorhombic structures for the compounds with $0.20 \le x \le 0.40$ were from synchrotron diffraction data. Structural parameters for compositions with $x < 0.2$ were obtained from laboratory X-ray data and are available from the authors. For $SrTi_{0.35}Zr_{0.65}O_3$ ($x = 0.35$), we observed an unusually large B value for the O(2) atoms (Table 1), the origin of which is unclear. However, given the insensitivity of X-ray diffraction to displacement of the light atoms this is most likely an artifact of the fitting procedure.

The refined structures were in reasonable agreement with that reported for $SrZrO_3$ (10, 11) with the expected small contraction in cell volume and M–O distances as the Ti content increased. In the case of $SrTi_{0.4}Zr_{0.6}O_3$ ($x = 0.40$), although the laboratory X-ray diffraction profile showed no reflections indicative of orthorhombic symmetry, such reflections were clearly evident in the synchrotron X-ray diffraction profile. This is a consequence of the narrower peaks and the higher signal-to-noise ratio in the synchrotron diffraction data.

Examples of the Rietveld plots from the synchrotron diffraction data are given in Fig. 2, illustrating the differences in the superlattice reflections between the orthorhombic *Pbnm* and tetragonal *I*4/*mcm* phases. These

[1] These superlattice reflections are due to cell enlargment as a result of tilting of the MO_6 octahedra. They are not a result of any B-site cation ordering in these oxides.

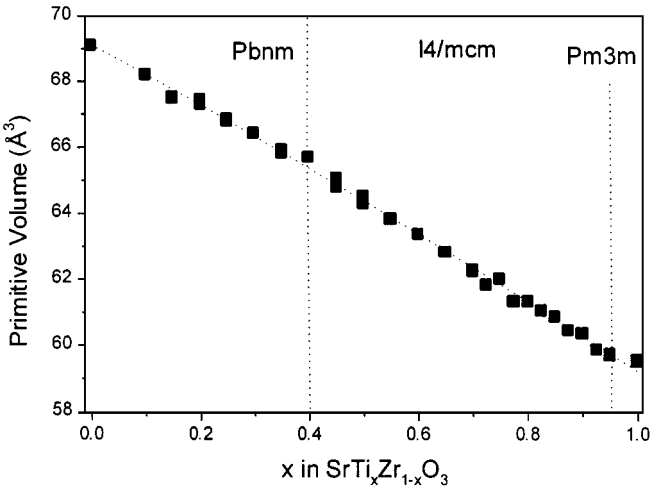

FIG. 1. Composition-dependent variation in the volume per formula unit for $SrTi_xZr_{1-x}O_3$.

distorted perovskites are characterized by tilting of the BO_6 octahedra and the phases are distinguished by differing tilt systems.

For samples with Ti contents greater than 40 mol%, (i.e., $x > 0.40$) the structure was found to be tetragonal in *I*4/*mcm*. This phase was studied by powder neutron diffraction methods using the MRPD. Neutron diffraction methods, being sensitive to the oxygen atoms, have a relative advantage in monitoring the tilting of the BO_6 octahedra. The 121 reflections (at $2\theta \approx 40°$) in the neutron diffraction profiles are good indicators of tetragonal symmetry. Based on the disappearance of the 121, and related, reflections in the neutron diffraction profiles, the transition from tetragonal *I*4/*mcm* to cubic $Pm\bar{3}m$ symmetry in $SrTi_xZr_{1-x}O_3$ occurs for $x > 0.95$ at room temperature (Fig. 3). The tetragonal structure is described by three structural parameters, a single variable O positional parameter u and the lattice parameters a and c. The results of the structural refinements from the powder neutron diffraction data are listed in Table 2, while examples of the fitted profiles are given in Fig. 4. Data for the cubic systems were satisfactorily reproduced with the ideal cubic structure.

The lower symmetry structures are also characterized by splitting of selected reflections. Such splitting is best observed using higher resolution synchrotron diffraction measurements. Synchrotron patterns showed well resolved splitting of the 202/022-type reflections in $SrZrO_3$. The magnitude of this decreased as Ti was added to the sample so that for the $x = 0.25$ sample there is no resolved splitting of these reflections, near $2\theta = 20°$ for $\lambda = 0.8$ Å. At this composition the synchrotron diffraction profiles still clearly showed the presence of superlattice reflections and these, rather than resolved splitting, are used to identify the crystal symmetry. We do not observe any *Cmcm* "marker"

TABLE 1
Lattice and Atomic Parameters Obtained from the Rietveld Refinements Using Synchrotron X-Ray Diffraction Data for Selected $SrTi_xZr_{1-x}O_3$ Samples

x		0.20	0.25	0.30	0.35	0.40	0.45	0.50
a (Å)		5.7512(1)	5.7318(1)	5.7238(2)	5.7039(1)	5.6977(1)	5.6910(2)	5.6753(2)
b (Å)		5.7640(1)	5.7391(1)	5.7258(2)	5.7192(1)	5.7154(1)	—	—
c (Å)		8.1335(1)	8.1216(1)	8.1049(1)	8.0748(2)	8.0697(1)	8.0329(3)	8.0131(4)
V (Å^3)		269.62(1)	267.17(1)	265.63(1)	263.42(1)	262.79(1)	260.03(1)	258.09(2)
Sr	x	− 0.0017(14)	0.0029(5)	− 0.0074(2)	0.0091(7)	− 0.004(16)	0	0
	y	0.5161(3)	0.5152(2)	0.5131(1)	0.5095(6)	0.5162(7)	$\frac{1}{2}$	$\frac{1}{2}$
	B (Å^2)	1.37(3)	1.06(2)	1.01(2)	2.26(10)	1.36(8)	1.11(1)	1.24(2)
Ti and Zr	B (Å^2)	0.56(3)	0.05(1)	0.05(1)	1.69(9)	1.10(9)	0.10(1)	0.19(2)
O(1)	x	− 0.0377(41)	− 0.0781(1)	− 0.0717(23)	− 0.0078(111)	− 0.0246(57)	0	0
	y	− 0.0019(23)	− 0.0090(14)	− 0.0062(13)	0.0044(38)	0.0174(44)	0	0
	B (Å^2)	1.79(30)	1.36(23)	3.88(36)	2.70(43)	1.04(40)	1.19(13)	1.97(28)
O(2)	x	0.2217(29)	0.2292(14)	0.2294(18)	0.2153(54)	0.2245(47)	0.2891(5)	0.2840(7)
	y	0.2821(27)	0.2782(14)	0.2748(16)	0.2112(53)	0.2346(44)	0.7891(5)	0.7840(7)
	z	0.0437(16)	0.0265(8)	0.0234(9)	− 0.0279(61)	0.0429(19)	0	0
	B (Å^2)	1.39(24)	0.09(9)	0.59(10)	8.46(79)	0.62(24)	1.10(8)	0.91(12)
R_p(%)		10.32	7.26	4.09	8.36	9.48	4.35	5.02
R_{wp}(%)		14.04	9.78	9.87	8.76	10.59	5.75	6.91
GOF		9.96	7.11	9.82	10.33	12.26	11.04	9.29

Note. The observed superlattice reflections are indicative of orthorhombic (*Pbnm*) structures at $x = 0.20$ to 0.40, and tetragonal ($I4/mcm$) at $x = 0.45$ and 0.50. In the *Pbnm* structure, the Sr occupies the 4*c* site at (x, y, $\frac{1}{4}$), and the Zr and/or Ti occupies the 4*a* site at (0, 0, 0). There are two types of oxygen atoms, O(1) on the 4*c* site at (x, y, $\frac{1}{4}$) and O(2) on the 8*d* site at (x, y, z). Details for the tetragonal structure are given in the caption for Table 2.

reflections, the 110, 112, 330, 114, and 332 peaks, in powder synchrotron or neutron profiles of the $x = 0.4$ sample. What is observed is a broadening of the reflections as the Ti content is increased. The (*Pbnm*) 222 reflection near 20° in the synchrotron diffraction profile of $SrTi_{0.25}Zr_{0.75}O_3$ has a FWHM of 0.078°. This width increases to 0.14° in $SrTi_{0.40}Zr_{0.60}O_3$ and 0.15 in $SrTi_{0.50}Zr_{0.50}O_3$. At still higher Ti contents the reflections renarrow, being 0.055° in $SrTi_{0.90}Zr_{0.10}O_3$. Since the samples were all annealed for prolonged periods and reannealing of selected samples failed to remove this broadening, this appears to be an intrinsic feature of the materials. The peak broadening can arise in a number of ways including compositional inhomogeneity and hysteresis near the phase transition. Since Zr^{4+} is appreciably larger that Ti^{4+} this size difference may also introduce some strain into the system and the associated broadening might be expected to be greatest at $x \approx 0.5$. As a consequence of the observed peak broadening it was not possible to use peak shapes to distinguish a *Cmcm* from a *Pbnm* structure.

Evidence for a *Cmcm* phase was then sought by cooling a tetragonal oxide with narrow diffraction peaks below room temperature. In general it was observed that for small tilt angles there was considerable uncertainty in estimating these using X-ray (including synchrotron) diffraction data. As a result of this observation, coupled with the small variation in the tilt angles on cooling from room temperature to 20 K, our discussion of these studies is brief. In the case of $SrTi_{0.9}Zr_{0.1}O_3$ the room temperature synchrotron diffraction pattern showed no clear evidence for any reflections indicative of tetragonal symmetry, although subsequent neutron diffraction measurements on the same sample clearly demonstrated the material to be tetragonal. On cooling below 200 K weak reflections indicative of tetragonal symmetry were observed and these increased slightly in intensity upon cooling. There was no evidence for additional reflections indicative of orthorhombic symmetry. The increase in intensity is, of course, a result of an increase in the tilting of the BO_6 octahedra upon cooling. A similar measurement was then conducted for $SrTi_{0.75}Zr_{0.25}O_3$. The pattern at 300 K showed clear evidence for a tetragonal structure, as was observed in the neutron diffraction study. On cooling, the intensity of the diagnostic superlattice reflections increased, indicating increased tilting of the BO_6 octahedra, although no additional reflections were observed, suggesting that the tetragonal structure persisted to 20 K. There was no evidence for any unusual changes in the peak shape or the lattice parameters upon cooling, suggesting that the symmetry remained the same and there is no evidence for the formation of a *Cmcm* intermediate phase near the $I4/mcm$–*Pbnm* phase boundary. We are continuing to study the nature of the structural transitions around the orthorhombic–tetragonal phase boundary in these and related systems.

The large difference in the size of the two tetravalent cations suggests the possibility of B-site cation ordering. In

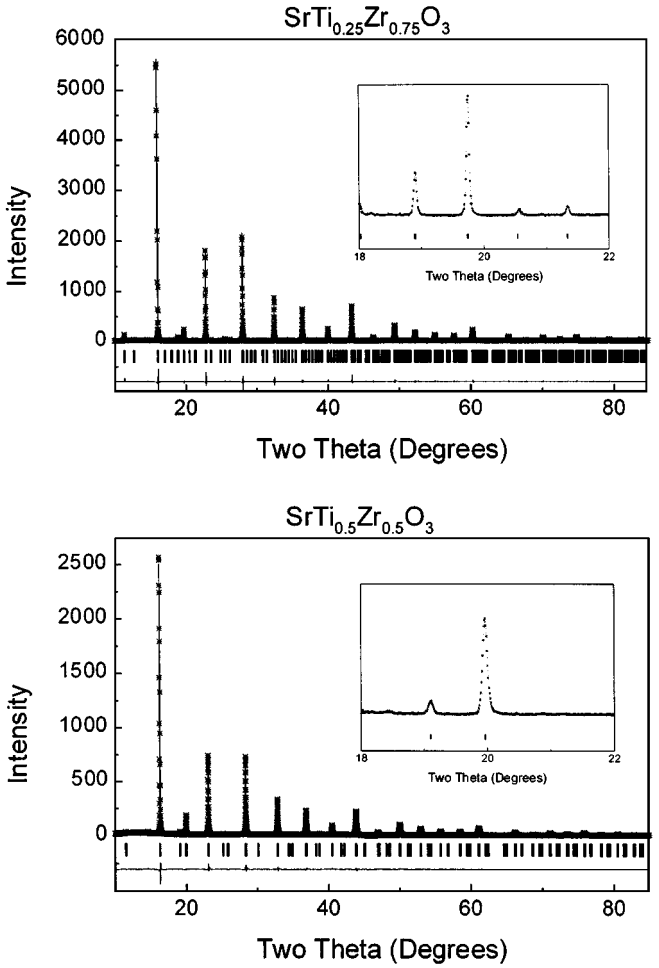

FIG. 2. Observed, calculated, and difference synchrotron diffraction profiles for $SrTi_{0.25}Zr_{0.75}O_3$ and $SrTi_{0.50}Zr_{0.50}O_3$. (Insets) Superlattice reflections indicative of orthorhombic symmetry in $SrTi_{0.25}Zr_{0.75}O_3$.

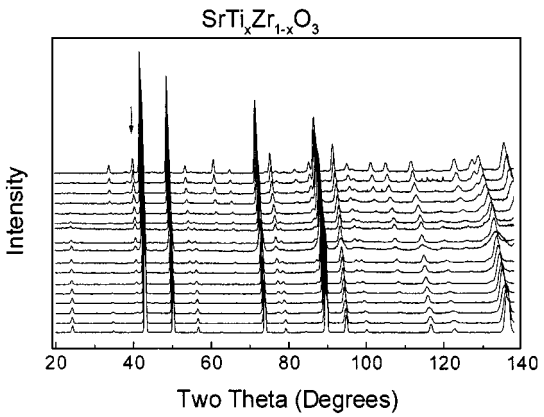

FIG. 3. Evolution in the powder neutron diffraction profiles upon increasing Ti content for $SrTi_xZr_{1-x}O_3$ for, from the top trace $x = 0.45$, 0.50, 0.55, 0.60, 0.65, 0.70, 0.725, 0.750, 0.775, 0.80, 0.825, 0.85, 0.875, 0.9, 0.925, 0.950, 0.975. The 121 reflection (arrowed in the top trace) is the most reliable indicator of tetragonal symmetry. The growth of the peak near $2\theta^\circ = 24^\circ$ is a consequence of the different signs of the scattering lengths of Ti (-0.3438 fm) and Zr (0.7160 fm).

order to examine this possibility in $SrTi_{0.5}Zr_{0.5}O_3$ ($x = 0.5$) the high-resolution powder diffractometer (HRPD) was used to collect an additional neutron diffraction data set. The structural refinements showed that $SrTi_{0.5}Zr_{0.5}O_3$ is tetragonal with *I*4/*mcm* symmetry, there being no evidence for cation ordering, that would also lower the symmetry. A similar conclusion could be reached from analysis of the synchrotron diffraction profiles.

Returning now to the obvious transitions. There are two additional points of note from the structural refinements:

1. The BO_6 octahedra are not rigid. Rather we observe that the B–O(2) distances are marginally longer than the B–O(1) distance so that the BO_6 octahedra are axially compressed, and the degree of this compression decreases as the transition to the cubic phase in approached (Fig. 5).

2. The interoctahedral B–O–B angles both gradually increase as the Ti content is increased and the slight difference between them becomes progressively smaller, indicative of a more regular structure at higher Ti contents. This is a result of a decrease in the tilting of the BO_6 octahedra at higher Ti contents.

These changes appear to be a feature of ABO_3-type perovskite oxides that are close to the *Pbnm*–*I*4/*mcm* boundary. In principle it is possible to estimate the magnitudes of the tilts for *rigid* BO_6 octahedra using the lattice parameters; however, our results clearly demonstrate that the octahedra are not rigid. Similar variations were observed in our variable temperature structural studies of $CaTiO_3$ and $SrMO_3$ (M = Zr, Hf, Ru). As in these previous studies we therefore prefer to estimate the tilt angles from the atomic coordinates.

The composition-induced transition from *I*4/*mcm* to $Pm\bar{3}m$ has been studied in considerable detail using powder neutron diffraction measurements and all the evidence indicates that it is continuous. The variations in the lattice parameters and the single variable oxygen position parameter show no measurable discontinuity. In the tetragonal phase the angle of rotation of the oxygen octahedron $\{\varphi = \tan^{-1} 4u\}$ can be taken as the order parameter. This tilt angle decreases steadily as the amount of Ti in the sample is increased, that is toward the cubic structure (Fig. 6). The temperature dependence of the tilt of the BO_6 octahedra in $PbTi_xZr_{1-x}O_3$ has been described using a generalized mean field treatment (24). The same model was used in this work except that the tilt angle becomes dependent on the composition rather than temperature. The tilt angle data were described by the function

$$\phi(x) = \eta(x)\phi(0),$$

TABLE 2
Lattice and Atomic Parameters Obtained from the Rietveld Refinements Using Neutron Diffraction Data for Tetragonal $SrTi_xZr_{1-x}O_3$ Samples

x		0.45	0.50	0.55	0.60	0.65	0.70	0.725	0.75	0.775	0.80	0.825	0.85	0.875	0.90	0.925	0.95
a(Å)		5.6812(5)	5.6650(6)	5.6517(7)	5.6418(8)	5.6232(6)	5.6073(7)	5.5945(6)	5.5997(9)	5.5803(5)	5.5794(5)	5.5722(5)	5.5665(4)	5.5550(5)	5.5509(3)	5.5367(6)	5.5254(7)
c(Å)		8.0298(7)	8.0110(9)	7.9911(10)	7.9647(11)	7.9411(10)	7.9206(11)	7.9022(9)	7.9150(12)	7.8786(9)	7.8800(10)	7.8667(9)	7.8579(8)	7.8354(10)	7.8370(7)	7.8140(11)	7.8232(20)
V(Å^3)		259.17(4)	257.09(5)	255.25(5)	253.51(6)	251.10(5)	265.62(6)	247.33(5)	248.20(6)	245.34(5)	245.30(5)	244.26(4)	243.49(3)	241.79(4)	241.45(3)	239.54(5)	238.84(7)
Sr	U_{11}	0.015(2)	0.009(2)	0.010(2)	0.010(1)	0.010(2)	0.017(2)	0.015(2)	0.023(2)	0.014(2)	0.016(4)	0.016(1)	0.010(1)	0.004(1)	0.003(1)	0.010(1)	−0.006(3)
	U_{33}	−0.002(2)	0.002(2)	−0.001(2)	0.001(1)	0.003(2)	−0.003(1)	−0.003(1)	−0.006(1)	−0.002(1)	0.015(3)	−0.004(1)	0.001(1)	0.005(1)	0.004(1)	−0.001(1)	0.009(4)
Ti and Zr	U_{11}	0.011(4)	0.041(3)	0.046(5)	−0.011(4)	0.054(126)	0.022(13)	0.001(6)	0.031(10)	0.002(4)	0.008(11)	0.010(3)	0.003(3)	0.002(3)	−0.001(3)	0.011(3)	−0.013(6)
	U_{33}	−0.001(3)	−0.019(1)	−0.018(3)	0.054(12)	0.200(199)	−0.033(39)	−0.028(3)	−0.026(13)	−0.019(3)	0.029(7)	−0.012(2)	−0.006(2)	−0.006(2)	−0.001(2)	−0.010(1)	0.010(9)
O(1)	U_{11}	0.026(2)	0.020(2)	0.030(3)	0.027(2)	0.014(2)	0.020(3)	0.030(3)	0.048(6)	0.020(3)	−0.002(3)	0.014(2)	0.012(2)	0.009(2)	0.005(3)	0.011(3)	−0.002(6)
	U_{33}	0.001(1)	0.006(1)	0.005(2)	−0.003(2)	−0.001(2)	−0.002(1)	−0.005(1)	0.003(4)	−0.003(1)	−0.004(1)	−0.001(1)	−0.001(1)	0.004(1)	0.002(1)	−0.001(1)	0.002(5)
O(2)	x	0.2832(3)	0.2814(3)	0.2782(4)	0.2775(4)	0.2769(2)	0.2747(4)	0.2723(4)	0.2715(6)	0.2698(4)	0.2698(3)	0.268(3)	0.2661(3)	0.2634(4)	0.2611(3)	0.2599(3)	0.2568(8)
	U_{11}	0.006(1)	0.006(1)	0.007(1)	0.012(1)	0.0005(1)	0.0050(1)	0.010(1)	0.007(2)	0.007(1)	0.004(2)	0.006(1)	0.005(1)	0.001(1)	0.003(1)	0.002(2)	−0.004(3)
	U_{33}	0.011(1)	0.009(1)	0.005(1)	0.004(1)	0.09(1)	0.0063(1)	0.002(1)	0.001(2)	0.003(1)	0.017(3)	0.004(1)	0.005(1)	0.007(1)	0.006(1)	0.004(1)	0.008(5)
	U_{12}	0.002(1)	0.003(1)	0.002(1)	−0.002(1)	0.002(1)	0.005(1)	−0.002(1)	0.001(2)	0.002(1)	−0.004(2)	−0.002(1)	0.000(1)	0.001(1)	0.001(1)	0.001(2)	0.002(3)
$(\phi)^\circ$		7.57(7)	7.16(8)	6.46(11)	6.30(8)	6.14(6)	5.63(8)	5.11(10)	4.86(14)	4.53(9)	4.13(16)	4.17(8)	3.69(6)	3.00(8)	2.64(8)	2.26(9)	1.54(18)
R_p(%)		3.16	3.48	3.31	3.43	3.06	3.09	2.99	3.77	3.27	3.11	2.85	3.01	3.9	2.91	4.1	3.40
R_{WP}(%)		3.91	4.31	4.33	4.31	3.78	4.03	3.71	4.87	4.15	3.96	3.66	4.15	5.06	3.75	5.34	4.71
GOF/χ^2		2.12	2.55	2.46	2.47	1.86	1.98	1.74	1.94	2.19	2.03	1.77	3.78	3.23	2.17	3.04	6.97
R_{Bragg}(%)		3.45	3.88	4.5	4.91	2.94	4.62	3.85	8.57	4.21	3.51	3.07	2.78	2.99	3.4	2.94	2.40

Note. In the $I4/mcm$ structure, the Sr occupies the 4*b* site at $(0, \frac{1}{2}, \frac{1}{4})$ and the Ti and/or Zr on the 4*c* sites at (0, 0, 0). There are also two types of oxygen atoms, O(1) on a 4*a* site at $(0, 0, \frac{1}{4})$ and O(2) on an 8*h* site at $(\frac{1}{4} + u, \frac{3}{4} + u, 0)$. The symmetry imposed constraints on the anisotropic thermal parameters (Å^2): Sr, Ti, Zr, and O(1) are $U_{11} = U_{22}$, and $U_{12} = U_{13} = U_{23} = 0$; O(2) is $U_{11} = U_{22}$, and $U_{13} = U_{23} = 0$.

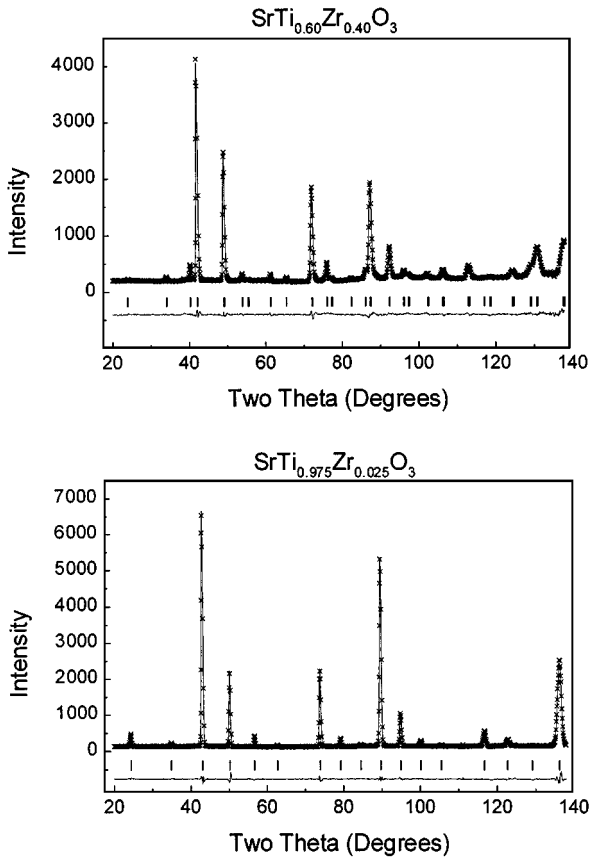

FIG. 4. Observed, calculated, and difference neutron diffraction profiles for $SrTi_{0.60}Zr_{0.40}O_3$ and $SrTi_{0.975}Zr_{0.025}O_3$. $SrTi_{0.975}Zr_{0.025}O_3$ is cubic and the structure was refined in space group $Pm\bar{3}m$ with $a = 3.9063(1)$ with standard R factors of R_p 3.83, R_{wp} 4.84, and R_B 2.87%. $SrTi_{0.60}Zr_{0.40}O_3$ is tetragonal and results of the structural refinement are given in Table 2.

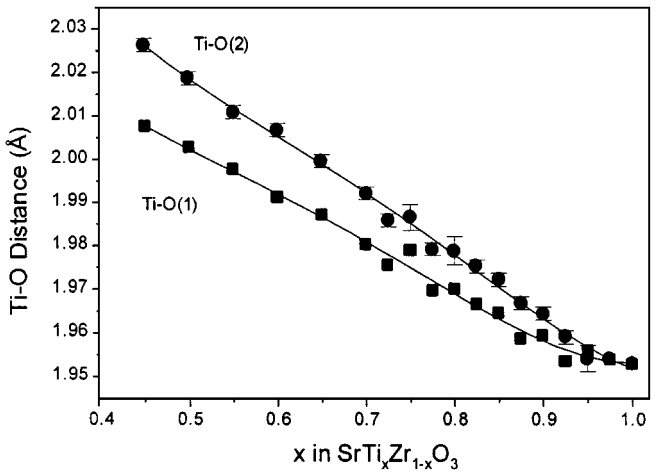

FIG. 5. Composition dependence of the B–O bond distances in $SrTi_xZr_{1-x}O_3$.

where $\phi(0)$ is the notional maximum angle of rotation, and $\eta(x)$ is the solution of the dimensionless equation:

$$\eta = \tanh\left[\frac{x_c}{x}\eta(1 + g_x\eta^2 + h_x\eta^4)\right].$$

In this equation, x is the mol% of the $SrTi_xZr_{1-x}O_3$, and x_c is the critical composition where the phase transition occurs. The values of g_x and h_x are constant (composition independent) coefficients. The observed oxygen tilt angles were well fitted by this function with the parameters $\phi(0) = 7.65^\circ$, $g_x = 0$, $h_x = -0.3$, and $x_c = 0.955$. The value of $\phi(0)$ gives a notional maximum angle of the BO_6 tilt in these tetragonal structures. The values for g_x and h_x correspond to a second-order transition (24). We have observed a similar continuous second order transition in the rhombohedral to cubic transition in $LaAlO_3$ (18).

Two room-temperature tetragonal samples were selected for additional high variable temperature studies, namely $SrTi_{0.5}Zr_{0.5}O_3$ and $SrTi_{0.75}Zr_{0.25}O_3$. Neutron powder diffraction data were recorded with increasing temperature. Examination of the observed neutron diffraction profiles demonstrated that both compounds undergo a transition from the tetragonal $I4/mcm$ to cubic $Pm\bar{3}m$ structure with increasing temperature. Figure 7 illustrates part of the powder neutron pattern for $SrTi_{0.5}Zr_{0.5}O_3$. Based on the disappearance of the superlattice reflections indicative of tetragonal symmetry, the tetragonal-to-cubic phase transition for $SrTi_{0.5}Zr_{0.5}O_3$ occurred between 948 and 998 K, whereas for $SrTi_{0.75}Zr_{0.25}O_3$ the phase transition occurred between 573 and 623 K. The refined structural parameters are given in Tables 3 and 4.

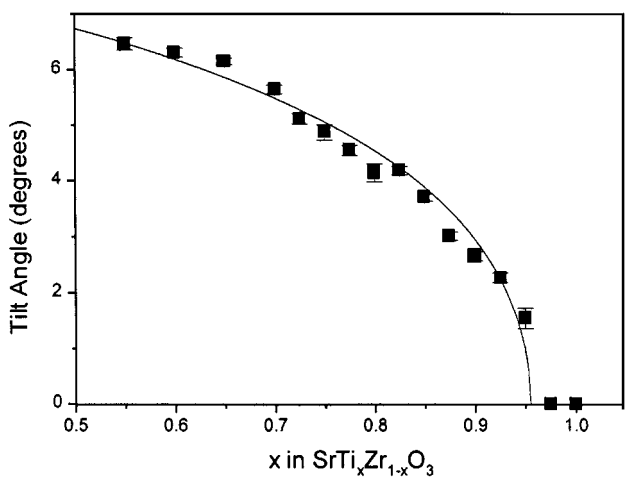

FIG. 6. Composition dependence of the rotations angle ϕ in the series of oxides $SrTi_xZr_{1-x}O_3$. The fitted line is given by $\phi(0) = 7.65^\circ$, $g_x = 0$, $h_x = -0.3$, and $x_c = 0.955$.

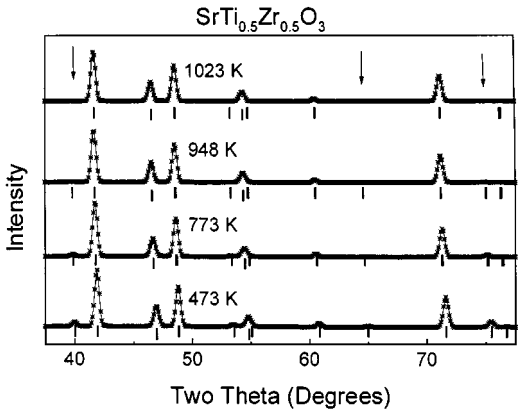

FIG. 7. Part of the powder neutron-diffraction profile showing the temperature dependence of some of the superlattice reflections. In each case the solid line is that calculated by the Rietveld refinement and the small vertical markers show the positions of all the allowed Bragg reflections.

For both $SrTi_{0.5}Zr_{0.5}O_3$ and $SrTi_{0.75}Zr_{0.25}O_3$ the BO_6 octahedra are axially compressed, with the longer B–O(2) distances being essentially independent of temperature, while the shorter B–O(1) distances increase smoothly, so that they become equal at the transition to the cubic structure (Fig. 8). In both cases there appears to be a slight discontinuity in the B–O distances near the transition point;

TABLE 3
Selected Structural Parameters and Bond Distance for $SrTi_{0.5}Zr_{0.5}O_3$

Temperature (K)	O(2) $(\frac{1}{4}+u)$	Tilt angle (°) $\phi=\tan^{-1}4u$	Bond distance (Å) Ti–O(1)	Ti–O(2)	Space group
473	0.2801(4)	6.865	2.0066(1)	2.0221(20)	*I*4/*mcm*
573	0.2782(4)	6.436	2.0082(2)	2.0231(20)	*I*4/*mcm*
623	0.2763(4)	6.005	2.0090(2)	2.0228(22)	*I*4/*mcm*
673	0.2748(4)	5.665	2.0107(1)	2.0227(24)	*I*4/*mcm*
698	0.2742(4)	5.529	2.0110(2)	2.0229(23)	*I*4/*mcm*
723	0.2731(4)	5.279	2.0113(2)	2.0231(25)	*I*4/*mcm*
748	0.2719(4)	5.006	2.0124(2)	2.0221(25)	*I*4/*mcm*
773	0.2707(5)	4.733	2.0126(2)	2.0229(27)	*I*4/*mcm*
798	0.2699(5)	4.551	2.0134(2)	2.0222(28)	*I*4/*mcm*
823	0.2675(5)	4.004	2.0137(2)	2.0215(27)	*I*4/*mcm*
848	0.2659(5)	3.639	2.0140(2)	2.0211(31)	*I*4/*mcm*
873	0.2638(4)	3.160	2.0146(2)	2.0204(24)	*I*4/*mcm*
898	0.2631(6)	3.000	2.0151(2)	2.0208(35)	*I*4/*mcm*
923	0.2616(7)	2.657	2.0155(2)	2.0206(38)	*I*4/*mcm*
948	0.2598(6)	2.245	2.0159(3)	2.0200(35)	*I*4/*mcm*
973	0.2572(8)	1.650	2.0159(2)	2.0201(45)	*I*4/*mcm*
998	—	—	2.0178(1)	—	$Pm\bar{3}m$
1023	—	—	2.0180(1)	—	$Pm\bar{3}m$

Note. The numbers in parenthesis are the esds. The cubic structures were refined in space group $Pm\bar{3}m$ where the Ca is on the 1*b* site at $(\frac{1}{2},\frac{1}{2},\frac{1}{2})$ the Ti the 1a site at (0, 0, 0) and the O the 3*d* site at $(\frac{1}{2},0,0)$. Details for the tetragonal structure are given in Table 2.

TABLE 4
Selected Structural Parameters and Bond Distances for $SrTi_{0.75}Zr_{0.25}O_3$ ($x=0.75$).

Temperature (K)	O(2) $(\frac{1}{4}+u)$	Bond distance (Å) Ti–O(1)	Ti–O(2)	Space group
373	0.2717(3)	1.9754(2)	1.9856(19)	*I*4/*mcm*
473	0.2670(5)	1.9773(2)	1.9855(30)	*I*4/*mcm*
523	0.2649(5)	1.9789(2)	1.9854(28)	*I*4/*mcm*
573	0.2616(5)	1.9801(2)	1.9852(27)	*I*4/*mcm*
583	0.2604(5)	1.9806(2)	1.9849(30)	*I*4/*mcm*
593	0.2602(6)	1.9804(2)	1.9853(34)	*I*4/*mcm*
603	0.2585(7)	1.9808(2)	1.9849(37)	*I*4/*mcm*
613	0.2580(7)	1.9811(2)	1.9851(38)	*I*4/*mcm*
623	—	1.9820(1)	—	$Pm\bar{3}m$
633	—	1.9832(1)	—	$Pm\bar{3}m$
643	—	1.9833(1)	—	$Pm\bar{3}m$
653	—	1.9835(1)	—	$Pm\bar{3}m$
663	—	1.9838(1)	—	$Pm\bar{3}m$
673	—	1.9842(1)	—	$Pm\bar{3}m$

Note. The numbers in parenthesis are the esds.

however, this most probably reflects problems in accurately determining both the tetragonal c/a ratio and the oxygen positional parameter at temperatures just below the transition. In the absence of observed splitting of the strong reflections the c/a ratio is also obtained from the weak superlattice reflections.

The temperature dependent variation in the tilt angle was reproduced using the original mean field expression (24) in which T_c is the phase transition temperature. For $SrTi_{0.5}Zr_{0.5}O_3$ the optimal parameters were $\phi(0)=7.4°$, $g_T=0$, $h_T=-0.35$, and $T_c=983$ K; whereas for $SrTi_{0.75}Zr_{0.25}O_3$ $\phi(0)=6.0°$, $g_T=0$, $h_T=-0.41$, and $T_c=622$ K (Fig. 9). Again the values of g correspond to

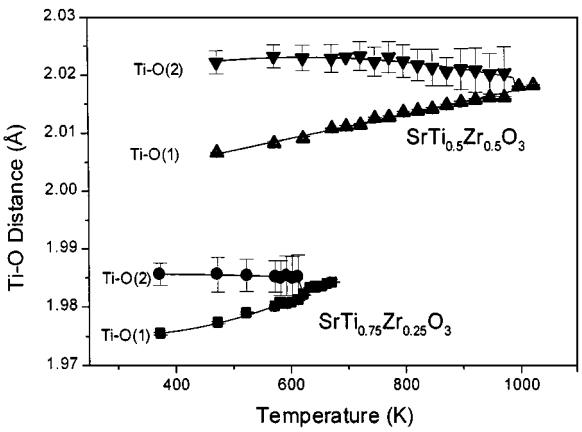

FIG. 8. Temperature dependence of the B–O bond distances in $SrTi_{0.50}Zr_{0.50}O_3$ and $SrTi_{0.75}Zr_{0.25}O_3$.

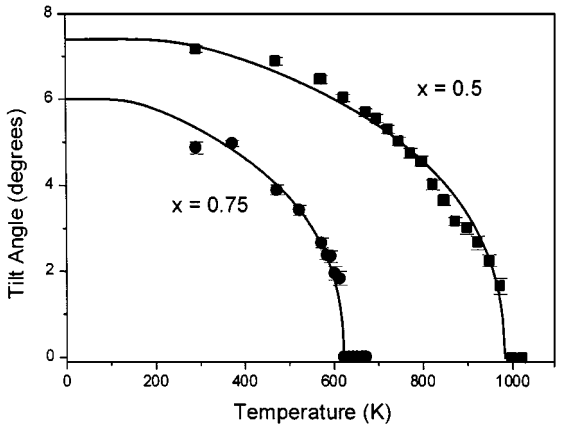

FIG. 9. Temperature dependence of the rotations angles, ϕ, in $SrTi_{0.50}Zr_{0.50}O_3$ and $SrTi_{0.75}Zr_{0.25}O_3$. The fitted lines are given by $\phi(0) = 7.4^\circ$, $g_T = 0$, $h_T = -0.35$, and $T_c = 983$ K for $SrTi_{0.5}Zr_{0.5}O_3$ and by $\phi(0) = 6.0^\circ$, $g_T = 0$, $h_T = -0.41$, and $T_c = 622$ K for $SrTi_{0.75}Zr_{0.25}O_3$.

a continuous second-order transition. The fitting suggests that the maximum angles of the BO_6 tilt in $SrTi_{0.5}Zr_{0.5}O_3$ and $SrTi_{0.75}Zr_{0.25}O_3$, are 7.4° and 6.0°, respectively. The notional maximum tilt of the BO_6 octahedra is smaller in $SrTi_{0.75}Zr_{0.25}O_3$ than in $SrTi_{0.5}Zr_{0.5}O_3$. These two values are intermediate between the tilts observed in $SrTiO_3$, where $\phi(0) = 2.1^\circ$, and $SrZrO_3$, where $\phi(0) = 8.0^\circ$. It appears that the tilt angle at room temperature makes a good predictor of the transition temperature.

CONCLUSION

A series of *B*-site doped perovskite $SrTi_xZr_{1-x}O_3$ ($x = 0$ to 1) were prepared and structurally characterized by X-ray and neutron powder diffraction methods. The sequence of structural transitions at room temperature with composition in $SrTi_xZr_{1-x}O_3$ was shown to be

$$\underset{\text{orthorhombic}}{x = 0} \quad \underset{\textit{Pbnm}}{\quad} \quad \underset{\longleftrightarrow}{x = 0.40} \quad \underset{\text{tetragonal}}{\quad} \quad \underset{\textit{I4/mcm}}{\quad} \quad \underset{\longleftrightarrow}{x = 0.95} \quad \underset{\text{cubic}}{\quad} \quad \underset{\textit{Pm}\bar{3}\textit{m}}{\quad} \quad x = 1.$$

There is no evidence for the presence of either a second orthorhombic (*Cmcm*) phase or of ordering of the Zr and Ti cations.

The structural transition from tetragonal to cubic symmetry involves tilts of the BO_6 (B = Ti or Zr) octahedra. Similar changes occur with increase in either the Ti content or the temperature. The tilt angle of the compound decreases as the Ti composition (x) increases. The evolution of the tilt of the BO_6 octahedra has been well described using a generalized mean field treatment. This work represents the most comprehensive study of the phase transitions in a *B*-site doped perovskite system showing both the composition- and the temperature dependence and clearly demonstrates the complementary nature of these two effects.

ACKNOWLEDGMENTS

This work has been supported by The Australian Research Council and The Australian Institute of Nuclear Science and Engineering. Part of this work was performed at the Australian National Beamline Facility with support from the Australian Synchrotron Research Program, which is funded by the Commonwealth of Australia under the Major National Research Facilities program. Brookshaven National Laboratory is operated by Brookhaven Science Associates for the U.S. Department of Energy under Contract DE-AC02-98-CH10886.

REFERENCES

1. M. A. Carpenter and E. K. H. Salje, *Eur. J. Miner.* **10,** 693 (1998).
2. A. E. Ringwood, S. E. Kesson, K. D. Reeve, D. M. Levins, and E. J. Ramm, *in* "Radioactive Waste Forms for the Future" (W. Lutze and R. C. Ewing, Eds.), p. 233. Elsevier, Amsterdam, 1988.
3. B. Raveau, C. Michel, M. Hervieu, and D. Groult, "Crystal Chemistry of High T_c Superconducting Copper Oxides." Springer-Verlag, Berlin, 1991.
4. S. Jin, T. H. Tiefel, M. McCormack, R. A. Fastnacht, R. Ramesh, and L. H. Chen, *Science* **264,** 4113 (1994).
5. L. E. Cross, *Ferroelectrics* **151,** 305 (1994).
6. D. L. Corker, A. M. Glazer, J. Dec, K. Roleder, and R. Whatmore, *Acta Crystallogr. B* **53,** 135 (1998).
7. C. J. Ball, B. D. Begg, D. J. Cookson, G. J. Thorogood, and E. R. Vance, *J. Solid State Chem.* **139,** 238 (1998).
8. G. Shirane and Y. Yamada, *Phys. Rev.* **177,** 858 (1969).
9. B. J. Kennedy, C. J. Howard, and B. C. Chakoumakos, *J. Phys. C. Condens. Matter* **11,** 1479 (1999).
10. B. J. Kennedy, C. J. Howard, and B. C. Chakoumakos, *Phys. Rev. B* **59,** 4023 (1999).
11. A. Ahtee, M. Ahtee, A. M. Glazer, and A. W. Hewat, *Acta Crystallogr. B* **32,** 3243 (1976).
12. M. Ahtee, A. M. Glazer, and A. W. Hewat, *Acta Crystallogr. B* **34,** 752 (1978).
13. B. J. Kennedy, C. J. Howard, and B. C. Chakoumakos, *Phys. Rev. B* **60,** 2972 (1999).
14. P. M. Woodward, *Acta Crystallogr. B* **53,** 44 (1997).
15. C. J. Howard and H. T. Stokes, *Acta Crystallogr. B* **54,** 782 (1998).
16. B. J. Kennedy, A. K. Prodjosantoso, and C. J. Howard, *J. Phys. C. Condens. Matter* **11,** 6319 (1999).
17. B. J. Kennedy and B. A. Hunter, *Phys. Rev. B* **58,** 653 (1997).
18. C. J. Howard, B. J. Kennedy, and B. C. Chakoumakos, *J. Phys. C. Condens. Matter* **12,** 349 (2000).
19. T. M. Sabine, B. J. Kennedy, R. F. Garrett, G. J. Foran, and D. J. Cookson, *J. Appl. Crystallogr.* **28,** 513 (1998).
20. G. C. Smith, *Synchrotron Radiat. News* **4,** 24 (1991).
21. S. J. Kennedy, *Adv. X-Ray Anal.* **38,** 35 (1995).
22. C. J. Howard, C. J. Ball, R. L. Davis, and M. M. Elcombe, *Aust. J. Phys.* **36,** 507 (1983).
23. C. J. Howard and B. A. Hunter, "A Computer Program for Rietveld Analysis of X-ray and Neutron Powder Diffraction Patterns," pp. 1–27. Lucas Heights Research Laboratories, 1998.
24. N. Cereceda, B. Noheda, T. Iglesias, J. R. Ferández-del-Castillo, J. A. Gonzalo, N. Duan, Y. L. Wang, D. E. Cox, and G. Shirane, *Phys. Rev. B* **55,** 6174 (1997).